Benchmarking of strength models for unidirectional composites under longitudinal tension

Anthony Bunsell[a], Larissa Gorbatikh[b], Hannah Morton[c], Soraia Pimenta[d,*], Ian Sinclair[c], Mark Spearing[c], Yentl Swolfs[b], Alain Thionnet[a,e]

[a]*Mines ParisTech, PSL Research University, Centre des Matériaux, CNRS UMR 7633, BP 87, 91003 Evry, France*
[b]*Department of Materials Engineering, KU Leuven, Kasteelpark Arenberg 44, 3001 Leuven, Belgium*
[c]*Material's Research Group, University of Southampton, University Road, Southampton SO17 1BJ, United Kingdom*
[d]*Dept Mechanical Engineering, South Kensington Campus, Imperial College London, SW7 2AZ, United Kingdom*
[e]*Université de Bourgogne, Bâtiment Mirande, BP 47870, Dijon, France*

Abstract

Several modelling approaches are available in the literature to predict longitudinal tensile failure of fibre–reinforced polymers. However, a systematic, blind and unbiased comparison between the predictions from the different models and against experimental data has never been performed. This paper presents a benchmarking exercise performed for three different models from the literature: (i) an analytical hierarchical scaling law for composite fibre bundles, (ii) direct numerical simulations of composite fibre bundles, and (iii) a multiscale finite–element simulation method. The results show that there are significant discrepancies between the predictions of the different modelling approaches for fibre–break density evolution, cluster formation and ultimate strength, and that each of the three models presents unique advantages over the others. Blind model predictions are also compared against detailed computed–tomography experiments, showing that our understanding of the micromechanics of longitudinal tensile failure of composites needs to be developed further.

Keywords: A. Polymer–matrix composites, B. Fragmentation, B. Strength, C. Micro-mechanics.

1. Introduction

Composites are a rapidly growing class of materials for lightweight, high-performance applications. However, composite components are often overdesigned, which leads to sub-optimal performance and hence larger and heavier parts. A reason for this overdesign is the lack of reliable predictive models for the mechanical response of composite materials, which is directly linked to an incomplete understanding of their failure mechanisms. Since composites consist of reinforcing fibres inside a

*Corresponding author.
Email addresses: anthony.bunsell@mines-paristech.fr (Anthony Bunsell), larissa.gorbatikh@kuleuven.be (Larissa Gorbatikh), h.morton@soton.ac.uk (Hannah Morton), soraia.pimenta@imperial.ac.uk (Soraia Pimenta), i.sinclair@soton.ac.uk (Ian Sinclair), s.m.spearing@soton.ac.uk (Mark Spearing), yentl.swolfs@kuleuven.be (Yentl Swolfs), alain.thionnet@mines-paristech.fr alain.thionnet@u-bourgogne.fr (Alain Thionnet)

matrix, their behaviour is not only governed by these two constituents but also by the interactions between them. This makes predicting the mechanical behaviour of composites inherently complex.

An essential part of advancing state–of–the–art material models is to compare their predictions against experimental data. This principle was embraced by a series of three World Wide Failure Exercises [1–5]. The overall goal of these exercises was to provide an objective assessment of different failure criteria for fibre–reinforced composites in complex 3D stress states. These efforts were spread over many years, involved many participants, and required complex experiments. Overall, the results were enlightening, with the main conclusions being:

- Detailed and quantitative comparisons between the models led to identification of the fundamental mechanisms that each model should ideally capture. This should catalyse and streamline progress in the field;
- The models required a large number (20–80) of input properties, some of which were difficult to measure. Also, some degree of parameter–fitting was unavoidable in some cases;
- Even the best models were not able to capture the experimental results with the accuracy required for model–based structural design. This was ascribed to a combination of the complex loading scenarios and the multidirectional nature of the composites. In some cases, it was found likely that the lack of agreement between models and experiments was due to experimental issues.

The World Wide Failure Exercises benchmarked models for predicting the response of complex, multidirectional composites under complex 3D stress states using the basic mechanical properties of unidirectional plies as inputs. Another important and challenging problem for designing composite materials and structures is predicting the basic mechanical properties of unidirectional composite plies using the properties of their constituents (fibres, matrix and interfaces) as inputs. Amongst all basic mechanical properties of unidirectional composite plies, the longitudinal tensile strength is one of the most critical for the reliability of composite structures, as longitudinal tensile failure of one composite ply often triggers the ultimate failure of the entire structure.

The longitudinal tensile failure process of unidirectional composites is relatively well understood, as nearly all researchers agree on the fundamental governing mechanisms. As the composite is loaded along the fibre–direction, the weakest fibres will fail first, which will cause them to lose their load carrying capacity over a certain length. The load of a broken fibre is shed to the nearby fibres, which are hence subjected to stress concentrations; this increases their failure probability, and causes a tendency to develop clusters of fibre–breaks, which increases stress concentrations even further. At some

point, one cluster will become so large that it starts growing unstably; this critical cluster will cause final failure of the composite.

In the light of this common understanding, longitudinal tensile strength models are therefore a combination of two key concepts: (i) the single–fibre strength distribution and (ii) the stress concentrations around broken fibre(s). These two key concepts have been formulated and implemented in fundamentally different ways in various models since the 1950s, as detailed in several reviews available in the literature [6–8]; however, these different models have not been thoroughly benchmarked against each other, nor against independently obtained blind–experiments. Consequently, there is currently no way to truly compare or assess different modelling approaches in terms of (i) the relative importance of the different features considered, (ii) the balance between accuracy and computational cost, and (iii) their predictive capabilities.

Also, as detailed in a recent review paper [8], many longitudinal tensile strength models in the literature have been positively validated against experiments, with reported prediction errors below 20% [9–15]. However, this may be not representative of their true predictive capability, due to (at least) three reasons. Firstly, model validation is usually conducted against a small number of experiments whose results are known *a priori*, and which are often conducted alongside model development; this means that models are developed further until they correlate well with that particular set of experiments, leading to confirmation bias. Therefore, it is vital to compare blind model predictions against experiments, in order to avoid confirmation bias and truly assess the accuracy of the models.

Secondly [8], the strength of individual fibres is a stochastic variable; to obtain a reliable Weibull distribution, a simple statistical simulation can show that hundreds of tests are needed [16, 17]. With the 25–100 fibres that most authors test (considering only one gauge length), the uncertainty in the predicted strength of a composite is estimated to be at least 10% [16]. This however assumes flawless experiments, so adding experimental errors and the uncertainty on matrix properties is likely to decrease the accuracy of model predictions further.

Thirdly, different modelling assumptions and approaches should intrinsically lead to predictions with different levels of accuracy. Moreover, models consider much simpler microstructures (e.g. perfectly–parallel and straight fibres, homogeneous matrix, amongst other simplifications) than those experimentally observed in composites [18]. This means that, if model predictions match experimental results perfectly, the models must be accounting for these differences through non-physically–based features, intentionally or otherwise. This highlights that there are gaps in our knowledge which need to be addressed.

The field of longitudinal tensile failure of unidirectional composites therefore needs a benchmarking exercise similar to the World Wide Failure Exercises. This should focus not only on assessing predictive capabilities of the different models, but also — and most importantly — on assessing our understanding of longitudinal tensile failure mechanisms, examining the effect of different model assumptions and methodologies, and identifying gaps in both models and experiments.

This paper describes the first version of such an exercise, as detailed in Sections 2 and 3. Section 4 summarises the three different models included in this exercise, and Section 5 describes the experiments performed independently to validate blind predictions; while those models have been published elsewhere [14–16, 19–28] and the experiments applied previously–published methods [23, 29, 30], this work is original in that it provides the first comparison between blind model predictions and experiments (focusing not only on final failure but also on progressive damage accumulation), and also the first comprehensive comparison in the literature between three independently–developed models. Results are presented in Section 6 and discussed in Section 7, with the main conclusions summarised in Section 8.

2. Overview of the benchmarking exercise

2.1. Objectives

The aim of this benchmarking exercise was to compare the predictions of different models for the longitudinal tensile failure of unidirectional composites, not only against each other but also with experimental data. This comparison focused on the tensile strength and the accumulation of fibre–breaks in unidirectional composites under quasi-static longitudinal tension, applied as a uniform and monotonic stress or displacement far–field.

The benchmarking exercise was proposed and carried out considering that the different models in the literature present unique combinations of advantages and shortcomings, and are applicable under distinct conditions. Consequently, instead of aiming to rank the models according to their quantitative performance, this exercise had the following objectives:

i. Comparing model predictions with experimental data, both in terms of ultimate failure and accumulation of fibre breaks;
ii. Establishing benefits and drawbacks of the different models;
iii. Establishing gaps in literature and aspects requiring future improvements.

2.2. Organisation, timeline and contributors to the exercise

The benchmarking exercise analysed the longitudinal tensile failure of two Fibre–Reinforced Polymers (FRPs):

Case I: a hypothetical composite for which the model inputs provided did not correspond to any factual experimental data. Consequently, there was no experimental data to benchmark the predictions from the models, nor any indication of the expected results, making Case I suitable for a truly–blind comparison between the participating models;

Case II: an actual high–performance carbon/epoxy system (with T800 fibres and M21 matrix), with modelling inputs collected from the literature. For the T800/M21 material system, most of the required model outputs had not been experimentally measured in the literature, and experiments were therefore carried out specifically for the purpose of this exercise; the experimental results were disclosed to the modelling participants (see Table 1) only after the modelling predictions were circulated.

The benchmarking exercise was organised and ran according to the following timeline:

1. A document defining the scope of the benchmarking exercise, the instructions to participants, and the modelling inputs was drafted, revised and agreed between all participants in June 2014. The invitation to participate in the exercise was sent to eleven research groups with published models for predicting tensile failure of composites; five of these groups accepted to participate in the exercise;

2. Modelling predictions were prepared according to the instructions, and circulated amongst the participants in November 2014. Four research groups submitted modelling predictions;

3. The experimental results were finally disclosed to the modelling participants in December 2014;

4. The results (modelling and experimental) were collated and circulated to all participants in February 2015, after which the participants met to discuss the outcomes of the benchmarking exercise. Three research groups that contributed with modelling predictions and the research group that contributed with experimental data agreed to prepare this joint publication on the benchmarking exercise.

Table 1 provides an overview of the participants that contributed to the benchmarking exercise and to this publication.

3. Definition of case–studies and inputs provided to participants

3.1. Case I: failure and damage accumulation in a hypothetical composite

Case I analyses a hypothetical composite with isotropic fibre and matrix properties shown in Table 2. The provided inputs do not correspond to any existing fibre/matrix system, hence one objective of Case I was to compare truly blind predictions from the different models against each other, since there was no indication of the expected results. Moreover, the inputs selected for Case I were significantly different from those in Case II; this will allow us to distinguish between (i) *systematic* differences between the predictions of the participating models due to their *intrinsic assumptions*, and (ii) *coincidental* differences between the predictions of the participating models due to the *particular set of inputs* used.

As model results, a minimum of 10 realisations were requested for the following outputs:

- Full stress–strain curves;
- Failure strain and strength;
- Density of fibre breaks (breaks per volume) vs. applied strain;
- Size of largest cluster vs. applied strain.

3.2. Case II: failure and damage accumulation in a carbon/epoxy (T800/M21) material

Case II aimed to compare blind model predictions for a real carbon/epoxy composite (T800/M21) against experimental data. The micromechanical inputs required to run the models are shown in Table 3; the values were collected from the literature as follows:

- Fibre geometry and elastic constants: the diameter and longitudinal Young's modulus were taken from the manufacturer's datasheet [31], and the other elastic constants were taken from the inputs to the Third World Wide Failure Exercise [32] (assuming transverse isotropy). While there is a significant uncertainty associated with the values used for the transverse elastic properties of the fibres, this uncertainty is expected to have a negligible effect on the predictions from all models considered;

- Fibre strength distribution: this was assumed to follow a simple Weibull distribution, with parameters measured by Tanaka et al. [33] through a combination of 200 single–fibre tensile tests (performed at four different gauge lengths) and 15 single–fibre fragmentation tests (each registering at least 10 fibre–breaks; this should provide a reasonably accurate (from a statistical point of view) description of the single–fibre strength distribution. Nevertheless, the fibre strength distribution is arguably the most influential set of inputs for the models and, for this reason, the effect of considering other fibre strength distributions will be discussed in Section 7.3;

- Matrix/interface–dominated properties: these were based on the M21–matrix datasheet [34]. The interlaminar shear strength of T800/M21 provided in the datasheet (measured through three–point bending tests) was used; this was motivated by (i) the fact that the interlaminar shear strength combines contributions from both the matrix and fibre–matrix interfacial shear strengths (which are jointly responsible for the shear stress–transfer near fibre breaks), and (ii) well–known difficulties associated with the measurement of the actual *in situ* properties of the matrix on bulk polymer specimens [35, 36], especially for shear–related properties. The effect of considering a linear–elastic vs. an elastic–perfectly–plastic matrix constitutive law will be assessed through *direct numerical simulations* (see model description in Section 4.2), with results shown in Section 6; the influence of matrix/interfacial properties on the predictions of the models will be further discussed in Section 7.3;

- Composite geometry: the fibre volume fraction, specimen length and number of fibres within the experimental analysis window were measured by the University of Southampton and provided to the modelling participants.

The required outputs for Case II were the same as for Case I (see Section 3.1).

4. Overview of participating models

This section summarises the three models included in this exercise. Full details about each model are available in the references cited in the corresponding subsection, and Table 4 compares the main assumptions and features of the three models.

4.1. Hierarchical scaling law

The *hierarchical scaling law* is an analytical model to predict the strength distribution [14] and damage accumulation [24] in composite fibre–bundles; it builds up from previous work on the strength of *dry* hierarchical fibre–bundles [37], but adding shear–lag stress transfer to account for the presence of the matrix/interface [38], and considering that the ineffective length grows with the applied stress and with the number of fibres broken in a cluster [39]. The model pairs fibres into hierarchical fibre–bundles as shown in Figure 1a, and assumes that failure also propagates in a hierarchical and self–similar way; the mathematical description of the failure process in a level–[1] bundle (with two level–[0] fibres) is then extrapolated to describe the failure of a generic level–$[i+1]$ bundle (composed of two level–$[i]$ sub-bundles, each with a cross–section $A^{[i]}$ and perimeter $C^{[i]}$). Consequently, the survival probability ($S_{\mathrm{U,c}}^{[i+1]}$) of a level–$[i+1]$ bundle under a remote stress σ^{∞} is

calculated recursively from that of a level–$[i]$ bundle [14] as

$$S_{\mathrm{U,c}}^{[i+1]}(\sigma^{\infty}) = S_{\mathrm{U,e}}^{[i]}(\sigma^{\infty})^{4} + 2\cdot\left[1 - S_{\mathrm{U,e}}^{[i]}(\sigma^{\infty})^{2}\right]\cdot S_{\mathrm{U,e}}^{[i]}(\sigma^{\infty})\cdot S_{\mathrm{K,e}}^{[i]}(\sigma^{\infty})\,. \tag{1}$$

The first term on the right–hand–side of Equation 1 is the probability of the level–$[i+1]$ bundle surviving with no level–$[i]$ broken–clusters. The second term is the probability of the level–$[i+1]$ bundle surviving with one level–$[i]$ broken–cluster in the level–$[i+1]$ *control volume* $V_{\mathrm{c}}^{[i+1]}$; the latter is defined as the volume within which two level–$[i]$ breaks may interact through yielding of the matrix or of the fibre–matrix interface (with yielding shear stress $\tau_{\mathrm{m}}^{\mathrm{y}}$, taken here as the composite interlaminar shear strength), which is thus twice as long as the level–$[i]$ perfectly–plastic shear–lag *recovery length* l_{e} (as shown in Figure 1b). Consequently, the density of level–$[i]$ clusters in the composite is [24]

$$\hat{\rho}_{\mathrm{clust}}^{[i]}(\sigma^{\infty}) = \frac{2\cdot\left[1 - S_{\mathrm{U,e}}^{[i]}(\sigma^{\infty})^{2}\right]\cdot S_{\mathrm{U,e}}^{[i]}(\sigma^{\infty})\cdot S_{\mathrm{K,e}}^{[i]}(\sigma^{\infty})}{V_{\mathrm{c}}^{[i+1]}(\sigma^{\infty})}\,, \qquad \begin{array}{ll}\text{where} & V_{\mathrm{c}}^{[i+1]} = A^{[i+1]}\cdot 2\cdot l_{\mathrm{e}}^{[i]} \\ \text{and} & l_{\mathrm{e}}^{[i]} = \dfrac{2\cdot A^{[i]}}{C^{[i]}\cdot\tau_{\mathrm{m}}^{\mathrm{y}}}\cdot\sigma^{\infty}\,.\end{array} \tag{2}$$

The required level–$[i]$ survival probabilities under uniform stresses ($S_{\mathrm{U,e}}^{[i]}$) and linear stress concentrations ($S_{\mathrm{K,e}}^{[i]}$) are calculated from $S_{\mathrm{U,e}}^{[i]}$ through a generalised weakest link theory [14].

4.2. Direct numerical simulations

The *direct numerical simulation* method (see Figure 2) uses a Fibre–Bundle Model (FBM) similar to the spring element model [40] and has been extensively described in other publications [15, 16, 19–23]. Prior to each run of the FBM, the fibre locations are created and all fibres are divided into elements that have a length equal to the fibre radius. A Weibull strength is assigned to each element, corresponding to this length. The global strain is then gradually increased, after which the element stresses are calculated by multiplying the element strain by the fibre modulus. If the stress exceeds the strength in any of the elements, then that element is considered broken. The stress redistribution around the broken element is applied to all nearby elements based on Finite Element (FE) simulations. These FE simulations were run beforehand, and the output is transferred to the FBM using trend line equations. The FBM, therefore, exploits the benefits of the accuracy and detail of the FE simulations without the drawback of incurring the full computation cost of FE simulations each time that the FBM model is run. The FE simulations incorporated either an elastic or an elastic–perfectly–plastic matrix.

The application of the stress redistribution around a fibre–break occurs in two steps. The first step ignores any interactions between fibre–breaks, whereas the second applies a correction for interactions between the breaks. The superposition principle employed for this purpose has been described and validated elsewhere [15]. After applying these stress concentrations, additional fibre–breaks may

arise and the model hence checks for these occurrences. The FBM keeps on updating the stress redistribution until no new fibre–breaks are found within the strain increment. Then, the global strain is increased and the process repeats until final failure is detected. Final failure is established when the number of fibre–breaks within one strain increment increased exponentially, as this indicates the unstable growth of the critical cluster. At this point, the model is interrupted and all data is stored.

The model has been compared in detail with experiments [23] and has been extended to hybrid composites [16, 41]. Despite the complex microstructure and failure development in hybrid composites, it has successfully predicted the failure strain of carbon/glass hybrid composites [42].

4.3. Multiscale FE^2 model

The *multiscale FE^2 model* brings together literature work on the FE analysis of composites at the microscale [43, 44], time–dependent visco-elastic effects [45–47], and homogenisation methods [48]. The model was developed to allow FE calculations of long fibre composite structures, considering that the calculation cannot be made at the scale of the constituents (as the mesh would be too large) nor using a pure FE^2 process (as the calculation would be too long). Therefore, a simplified FE^2 multiscale approach [25–27] has been developed to overcome these limitations and find the failure point of a structure (Figure 3). The multiscale FE^2 process is *simplified* because the FE analysis is only used for the macroscopic (i.e. structural) scale, whereas the microscopic (i.e. fibre) scale makes use of a pre–calculated database [49–51].

The *multiscale FE^2 model* has been favourably compared with experimental tests made on specimens using acoustic emission [53, 54] and high resolution tomography [28] to monitor damage. The model has also been favourably compared to slow burst tests made on carbon–fibre composite pressure vessels [49]. Details of the modelling can be found elsewhere [49–51], but an overview is provided here.

The macroscopic scale works in the framework of Damage Mechanics and uses Representative Volume Elements (RVEs). The dimensions of the RVE (with 32 fibres and a length $L = 4$ mm) were selected by Blassiau [55] based on experimental and numerical work [56]. As a consequence, the *multiscale FE^2 model* cannot be used for structures having a volume smaller than one RVE.

The evolution of the state of an RVE is deduced from a database of FE simulations at the microscopic scale, where intact and broken fibres, matrix, and fibre/matrix interfaces (intact or debonded) are modelled explicitly. These simulations calculate the maximum overstress on intact fibres in RVEs with different configurations (i.e. different numbers of broken fibres, debonded lengths, fibre volume fractions, and matrix viscosity parameters), which are then are saved to a database [55, 57, 58]. The database was normalised by the elastic properties of the unidirectional composite, so it can be used for

other composites with elastic fibres and viscoelastic matrix without re-running the simulations (i.e. by re-scaling the results in the database according to the mechanical properties of fibres, mechanical properties of matrix, and fibre volume fraction).

Because the input data provided for this exercise (see Tables 2 and 3) specified specimen gauge–lengths below the RVE–length used in the *multiscale FE^2 model*, the *multiscale FE^2* simulations were run using longer (8 mm long) specimens; nevertheless, it was verified that this difference in modelled gauge–length should have no significant influence on the predictions.

5. Experimental procedures for Case II

5.1. Materials

The specimens tested experimentally for Case II were prepared as described by Swolfs et al. [23], but using T800 fibres in the present paper instead of T700. Hexcel HexPly T800/M21 carbon fibre/epoxy prepregs [34] were provided by Airbus UK, and stacked in a 1 mm thick $[90/0]_s$ layup. After autoclave curing, the composite had a fibre volume fraction of 55%. The specimens were water–jet cut to a 4 mm width, with a double–notch leaving a waisted region with a width of just 0.8 mm. The waisted cross–section of the specimens, therefore, contained close to 5500 fibres aligned with the load direction, and this cross–ply notched geometry has proven to be extremely convenient for gripping and imaging purposes [23, 29, 30, 59]. Previous research revealed that this procedure inflicted negligible damage to the specimens [29]. Aluminium end–tabs were glued to the specimen to reduce stress concentrations in the grips, and to facilitate the introduction of load. The nominal failure load was measured by testing ten specimens in a screw–driven load rig. Further details on this testing rig and methodology can be found in Wright et al. [29].

It must be noticed that, while the experiments were performed with *notched cross–ply specimens*, Case–II was modelled (by all three models in this exercise) as an *unnotched unidirectional* specimen with a cross section equal to the central 0°–ligament between the notches in the experimental specimen. However, previous studies [23, 28, 30, 59] have shown that, due to splitting of the 0°–plies at the notch roots and delaminations at the 0°/90° interfaces, the central 0°–ligament becomes decoupled from the surrounding material at approximately 70% of the failure load, *before* significant fibre breakage develops. Moreover, single fibre–breaks were found to be uncorrelated within that 0°–ligament, with no evidence of higher density of fibre–breaks near the roots of the notch [30, 59]; this supports the assumption that the notched geometry has little influence on the development of fibre–breaks.

5.2. Synchrotron radiation computed tomography

One specimen (prepared as described above, but not tested in the screw–driven rig) was tested using *in situ* synchrotron radiation Computed Tomography (CT) at the ID19 beam line at the European Synchrotron Radiation Facility (ESRF) in Grenoble, France. The voxel resolution was 1.4 μm, which was sufficient to allow use of an automatic fibre detection algorithm. This algorithm was further facilitated by using a propagation distance of 37 mm, which allowed a degree of near–field Fresnel edge enhancement. The tensile specimen was held at 4 different load levels for 2 min, and scanned over a length of 2.3 mm. However, the presence of the double notch caused all fibre breaks to occur within a length of 1.54 mm. This corresponds to a volume of 0.61 mm^3 for the 0° plies. This volume was used in the strength models as well as in the normalisation for the fibre break densities. The in-house software at ESRF was used for data reconstruction, whereas VG-Studio^{TM} and FIJI [60] were used for the analysis of fibre–breaks. All breaks were verified using visual inspection in at least two orthogonal planes to double–check the detection algorithm.

Clusters of broken fibres were identified considering that a cluster of n_{clust} fibre–breaks consists of n_{clust} neighbouring fibre–breaks with an axial separation smaller than 70 μm, which has previously been determined as a reasonable estimate of the characteristic stress transfer length for similar material systems [30].

6. Results from the benchmarking exercise

Figure 4 presents the predictions of the three models for the hypothetical composite in *Case I*, and Figure 5 compares the experimental results against model predictions for the T800/M21 composite in *Case II*. For both cases, the *direct numerical simulation* method considered two different matrix responses (either linear–*elastic* or elastic–perfectly–*plastic*).

The representative stress–strain curves shown in Figure 4c and Figure 5c were calculated differently by the three models: the curves from the *hierarchical scaling law* correspond to the expected strain for each applied stress up to expected failure; the curves from *direct numerical simulations* correspond to a representative run with failure strain similar to the average of 50 different runs; the curves from the *multiscale FE^2 model* correspond to the run of the model yielding the median strength. The initial stiffness considered by the *hierarchical scaling law* neglects the contribution of matrix tensile stresses to the overall composite stresses; *direct numerical simulations* account for the contribution of the matrix tensile stresses to the overall composite stresses through the rule–of–mixtures, while the *multiscale FE^2 model* does so via the microscopic FE simulation.

The calculation times shown in Figure 4d and Figure 5d correspond to (i) the total running time for the *hierarchical scaling law* , (ii) one run of the *direct numerical simulation* (excluding preliminary FE calculation of stress concentrations), and (iii) one run of the *multiscale FE^2 model* (excluding the generation of the microscale database, and using a macroscale model larger than the specimen specified in Tables 2–3, see Section 4.3).

The predicted evolution of (i) the density of breaks (shown in Figures 4e and 5e) and (ii) the size of largest cluster (shown in Figures 4f and 5f) were also calculated differently by the three models: the *hierarchical scaling law* results correspond to the expected statistical value of the number of fibre breaks and broken clusters; *direct numerical simulation* results correspond to the averaged fibre breakage for 50 different runs of the model; the *multiscale FE^2 model* results correspond to the realisation yielding the median strength.

Most of the relative trends between the predictions of the different models are similar in Cases I and II, showing that these trends result from intrinsic model assumptions rather than from the particular datasets of inputs considered. However, other trends differ between Case I and Case II, as will be discussed in Section 7.1.

7. Discussion

7.1. Comparison between predictions from the different models and against experimental results

Comparing the predictions obtained with the different models for the two cases considered (see Figures 4 and 5) reveals that:

a. The *hierarchical scaling law* and *multiscale FE^2 model* consistently predict lower strengths than *direct numerical simulations* (see Figures 4a and 5a), likely due to intrinsic model assumptions:

   i. The *hierarchical scaling law* assumes a constant stress concentration factor of $k = 2$ in the nearest neighbour, while *direct numerical simulations* and the *multiscale FE^2 model* use lower stress concentration factors estimated through FE. Moreover, the ineffective length near fibre–breaks grows with the applied stress and the cluster size in the *hierarchical scaling law*, contrary to *direct numerical simulations* and the *multiscale FE^2 model*. These two features lower the strength predicted by the *hierarchical scaling law* when compared to *direct numerical simulations* and the *multiscale FE^2 model*;

   ii. The *multiscale FE^2 model* assumes that stress concentrations near fibre–breaks affect neighbouring fibres along (in the longitudinal direction) the entire length of the RVE — which is 4 mm long —, while the *hierarchical scaling law* and *direct numerical simulations*

assume that stress concentrations affect neighbouring fibres along (in the longitudinal direction) the corresponding recovery length (i.e. much more locally). Moreover, the *multiscale FE^2 model* modelled a larger specimen than the one considered in the experiments and by the other two modelling approaches. These two features lower the strength predicted by the *multiscale FE^2 model* when compared to the *hierarchical scaling law* and *direct numerical simulations*.

b. Figures 4c and 5c show that the *multiscale FE^2 model* predicts a significant amount of strain–softening before failure; this is due to (i) the progressive accumulation of *co-planar* fibre breaks, and (ii) the fact that the loss of longitudinal stiffness in the entire 4 mm length of each RVE is proportional to the number of fibre–breaks in that RVE. In contrast, the *hierarchical scaling law* predicts a very limited amount of non-linearity, and the *direct numerical simulation* method assumes a linear–elastic response for the composite (alternatively, *direct numerical simulations* are also capable of accounting for a non-linear response of the fibres [23]).

c. Figure 4c also highlights that the *direct numerical simulations* and *multiscale FE^2 model* account for the contribution of the stiffness of the matrix to the overall stresses and Young's modulus of the composite, while the *hierarchical scaling law* neglects this contribution. This difference is noticeable in the stress–strain curves predicted for Case I (hypothetical material, Figure 4c) but not for Case II (T800/M21 carbon/epoxy, Figure 5c), due to the relatively similar Young's moduli of the fibres (100 GPa) and of matrix (10 GPa) used in the hypothetical case (see Tables 2 and 3).

d. The *hierarchical scaling law* and *direct numerical simulations* predict very similar evolutions of the overall density of fibre breaks with applied strain (see Figures 4e and 5e), while predictions of the *multiscale FE^2 model* are significantly different. From a failure–process point–of–view, this is because the overall fibre–break density is governed (in general) by individual breaks [24, 30], which are defined only by the statistics of fibre strength (and which are the same in the *hierarchical scaling law* and *direct numerical simulations*, but different in the *multiscale FE^2 model*, as mentioned previously in point a.ii).

e. The very good agreement between the predictions for fibre–break density from the *hierarchical scaling law* and the *direct numerical simulations* is verified consistently for both sets of inputs used in Case I (Figure 4e) and Case II (Figure 5e), which is remarkable considering that they are calculated through completely different methods (the *hierarchical scaling law* uses purely–mathematical expressions as shown in Section 4.1, while the *direct numerical simulation* method determines the number of fibre–breaks explicitly). Moreover, the *multiscale FE^2 model* predicts

more fibre–breakage in Case I (Figure 4e) and less fibre–breakage in Case II (Figure 5e) than the other two models; this shows that the relative effect of different modelling approaches depends on the inputs used, and that the model which predicts the largest amount of fibre–breakage in one case may not do so consistently for a range of different inputs.

f. The clustering of fibre breaks predicted by the *multiscale FE^2 model* occurs faster than that predicted by the *hierarchical scaling law* and *direct numerical simulations*, for both Cases I (Figure 4f) and II (Figure 5f); this consistent difference is potentially due to the different size–effects on the single–fibre strength considered by the *multiscale FE^2 model* (see point a.ii above). The evolution of the largest cluster size with applied strain (Figures 4f and 5f) is consistently similar in the *hierarchical scaling law* and *direct numerical simulations* up to the formation of 2–plets (i.e. clusters with 2 fibre–breaks), but starts diverging once 4–plets are predicted by the *hierarchical scaling law* or observed experimentally; this suggests that the formation of small clusters (e.g. 2–plets) is governed by the single–fibre strength distribution, while the different stress concentration factors used by the two models only affect the formation of larger clusters, at larger applied strains.

g. At the failure point, the *hierarchical scaling law* predicts the smallest cluster of broken fibres of the models considered, consistently for both cases (Figures 4f and 5f). This is likely due to the hierarchical failure process considered (which models clusters as co–planar fibre breaks, leads to a stress concentration factor $k = 2$ in the nearest neighbour to a broken fibre/cluster, and accounts for the growing ineffective length with growing cluster size [39]).

h. Considering the overall predictions from the three different models, the best agreement in terms of failure strain and strength is seen between the *hierarchical scaling law* and the *multiscale FE^2 model*, while the best agreement in terms of accumulation and clustering of fibre breaks is seen between the *hierarchical scaling law* and *direct numerical simulations*. This shows that, due to the different modelling approaches, predictions for the progressive accumulation of fibre–breaks and for the final failure are not directly correlated, and that the ability of a model to predict failure correctly does not necessarily imply that the same model can predict accumulation of fibre–breaks accurately.

i. The *multiscale FE^2 model* predicts more non-linearity in the stress–strain curves (see Figures 4c and 5c) and the formation of larger clusters (see Figures 4c and 5c) than the *hierarchical scaling law* and *direct numerical simulations*, consistently for both Cases I and II; however, for Case II, the *multiscale FE^2 model* predicts the lowest density of fibre–breaks (Figure 5e) amongst all

models. This further shows that different modelling strategies may lead to significantly different relations between (i) the accumulation of fibre breaks, (ii) the formation of broken clusters, and (iii) the effect of fibre breakage on the overall stress–strain response of the composite predicted by the different models.

j. Considering plasticity of the matrix (as in the *hierarchical scaling law* and *direct numerical simulations* with *plastic* matrix) appears to be fundamental to predicting correct clustering of fibre breaks (Figure 5f); assuming an elastic matrix (as in *direct numerical simulations* with *elastic* matrix and in the *multiscale FE^2 model*) leads to predictions of much larger clusters of fibre–breaks than those observed experimentally.

k. The predictions from *direct numerical simulations* with a *plastic* matrix are, in general, closer to those from the *hierarchical scaling law* (also considering matrix plasticity) than to those from *direct numerical simulations* with an *elastic* matrix, even though the *hierarchical scaling law* and *direct numerical simulations* have very different modelling assumptions (e.g. regarding stress concentrations and clustering of fibre breaks). This shows that, while those assumptions are clearly affecting the results, the response assumed for individual fibres and the matrix is perhaps even more critical to the accuracy of the predictions.

7.2. Benefits and drawbacks of the different modelling approaches

The results from this exercise highlight the following benefits and drawbacks of each individual model:

- The *hierarchical scaling law* presents a very good agreement with experimental data (see Figure 5). Due to its analytical formulation, the *hierarchical scaling law* has a very low computational cost (running in less than one second, with no pre-processing required), which makes it scalable to very large structures. The most controversial feature of the *hierarchical scaling law* is the implied stress concentration factor $k = 2$, which overestimates the stress concentrations near individual fibre–breaks that have been calculated using static analyses of bundles with perfectly–aligned fibres [13, 20, 61]; however, stress concentrations $k \geq 2$ have been predicted for larger clusters (with 6 or more fibres) [62], and stress concentrations have a higher impact on the formation of large clusters than on the formation of small clusters (see Section 7.1.f.). Moreover, dynamic effects [63] and the random levels of fibre alignment in real composite microstructures [18] may lead to higher maximum values of stress concentrations than those predicted by existing FE models. This model is also the only one in this exercise that considers the effect of a growing ineffective length with larger clusters of broken fibres [39].

- The *direct numerical simulation* method uses less assumptions than the other models and has a greater versatility. At this point, features such as dynamic and viscoelastic effects, the increase in ineffective length with cluster growth, and fibre–matrix debonding have not been implemented yet, but its versatile framework makes these adaptations relatively straightforward. An important difference from the two other models is that it captures all possible cluster sizes, and hence allows for a more direct comparison with experimental data. The main drawback of the model is linked to the computational time and the largest bundle sizes that it can model. A multiscale framework based on an RVE could be built upon it to resolve this.

- The *multiscale FE^2 model* is the only one in this exercise that is implemented in a FE^2 simulation and can, therefore, be directly used to predict the response of both unnotched and notched structures, under non-uniform stress fields, and with multi-directional laminates; moreover, it is also the only model in this exercise that considers viscoelasticity of the matrix, and is therefore able to predict time–related effects (which, although not considered in this exercise, are important in other applications). However, this approach is not fully suitable to simulate structures smaller than the assumed RVE (with 32 fibres, 4 mm long), which was necessary in this exercise; moreover, the *multiscale FE^2 model* is conservative by design (e.g. it neglects the non-linear response of the matrix and assumes co-planar fibre–breaks), and it thus predicts the formation of larger broken–clusters and a more non-linear stress–strain response than those observed experimentally.

7.3. Open questions and gaps in the literature

The results presented in this paper show that further work is still required in several key areas, as discussed below.

More comprehensive datasets of experimental results for model validation. While the comparison between modelling and experimental results shown in Figure 5 is unquestionably valuable, a full validation of the predictive capabilities of models would require:

- Results from a number of nominally identical specimens rather than from a single specimen, to account for the variability associated with fibre strength, and to increase the representativeness of experimental data;

- Measuring the formation of fibre breaks in continuous tests, rather than having to interrupt the tests for 2 min at discrete load steps; such interruptions can lead to additional fibre breaks due to relaxation of the matrix, as previously shown by the *multiscale FE^2 model* (which considers visco–elastic matrix effects) [51];

- Measuring the density and clustering of fibre breaks along the entire loading history, in order to capture data at the end of the test (where most models start diverging);
- Including consistent variations of the same material (e.g. modifying the matrix, fibre–matrix interface, or fibre volume fraction while keeping the same fibre–type), to understand whether models can provide consistently good predictions for a range of materials.

More accurate inputs for material properties. The agreement between model predictions and experimental results can only be as good as the quality of the input properties. However, measuring data at the constituents level is intrinsically difficult:

- Regarding the single–fibre strength, there is still no universally accepted method to measure its statistical distribution accurately, as single–fibre tensile tests are inherently affected by stress concentrations at the grips [64], and single–fibre fragmentation tests require assumptions on the fibre–matrix stress transfer [65];
- There is also no agreement regarding whether the single–fibre tensile strength follows a simple Weibull distribution and the associated size effects (as assumed in inputs for Figures 4 and 5), or whether a different type of distribution is required [65, 66]. For instance, the failure strain predicted by *direct numerical simulations* for the T800/M21 case with *plastic* matrix drops from 3.00% to 2.56% if a bimodal Weibull distribution [65] is used instead of the default unimodal Weibull distribution; this bimodal distribution is based on exactly the same experimental data points as the unimodal distribution shown in Table 3, but fitted with a more advanced function. Similarly, *direct numerical simulations* predict a decrease in failure strain for the *elastic* matrix from 3.46% to 2.95% if the non-linear elasticity of carbon fibres is taken into account. This shows that the inputs characterising the response of single–fibres need to be measured accurately, as they have a significant effect on the predicted response of the composite;
- Regarding the properties of the matrix, it has been widely reported that they are size–dependent [35, 36] and, therefore, bulk matrix properties (especially strength) are unlikely to represent the actual *in situ* response of the matrix in a composite with large fibre–content. Also, detailed FE models (e.g. *direct numerical simulations*) require a plasticity/damage criterion to account for the *in situ* stress tri-axiality experienced by the matrix, for which there is no agreement in the literature either [67, 68]. The significant difference between the *elastic*– and *plastic*–matrix results of *direct numerical simulations* (Figures 4 and 5) strongly suggests that correctly capturing the overall matrix behaviour is vital. Nevertheless, for Case II, the *hierarchical scaling law* predicts that, once matrix plasticity is

considered, reducing the matrix shear strength by 50% would result in a 15% weaker composite, but with no significant effect on the accumulation and clustering of fibre–breaks (a further parametric study is reported in the literature [24]).

More insight on the interaction between fibre breaks and definition of clusters. The longitudinal tensile failure of unidirectional composites is governed not by individual fibre–breaks, but actually by the formation of clusters of interacting broken–fibres [30, 69]. Further work is thus required in order to:

- Provide an objective and unambiguous definition of what constitutes a cluster. At the moment, there are no sufficiently detailed studies defining the ineffective length of broken fibres or the threshold distance within which fibre–breaks interact, especially for larger clusters and in the bulk of real specimens with realistic fibre volume fractions and realistic matrix/interfacial constitutive laws (including matrix non-linearity, progressive matrix failure, and fibre–matrix debonding); consequently, different researchers use different definitions to identify clusters of fibre–breaks, which adds further uncertainty when comparing different models and experiments. This source of uncertainty could be overcome through *in situ* mapping of the full fibre or matrix stress/strain fields near fibre–breaks, at both the fibre and cluster scales; this mapping could ideally be done experimentally (e.g. using Raman spectroscopy) or, alternatively, through comprehensive finite element simulations;
- Obtain greater mechanistic insight into the dynamics of cluster formation. At the moment, the great majority of clusters appear instantaneously in the timescale that can be resolved by CT; complementary and correlated damage–event sensing that at least approaches stress–wave propagation times (e.g. via acoustic emission) would thus be required in order to identify the sequence of individual fibre–break events leading to cluster formation. This is particularly important because most direct numerical simulations tend to predict a more progressive formation of clusters than what is typically seen experimentally [8, 23]; this mismatch might be due to ignoring dynamic effects, as recent numerical simulations suggest that dynamic stress fields created during fibre–breakage are significantly different from those created under quasi-static conditions [70].

Defining the link between progressive damage accumulation and specimen failure. By the nature of the *in situ* CT observation of fibre breaks (with finite time–scales for imaging and small imaging volumes), it has not yet been possible to conclude whether ultimate failure results from the overall accumulation of fibre breaks and broken clusters distributed over a volume of mate-

rial, or from the formation of a critical cluster with a universal size. The fraction of broken fibres observed experimentally in specimens about to fail is relatively small ($\approx$ 10% in Figure 5e and in the literature [30]), which strongly suggests that clustering or localisation of fibre–breaks is key to triggering final failure. Most models (including those in this paper) assume a failure criterion driven by Strength of Materials, although the damage localisation phenomenon that is suggested in the CT experiments could also be predicted through Fracture Mechanics [69, 71]. More accurately determining the link between the damage state and the onset of tensile failure should be a key objective for the future development of models and experiments.

Accounting for more realistic microstructures. While some models can capture the effect of random fibre packings [20] and/or locally–varying fibre contents [50], the influence of larger–scale defects has not been studied yet. However, the actual microstructure of FRPs has a very complex geometry and topology [18] — with fibre waviness and entanglement, presence of voids, large resin rich regions — which is likely to affect the longitudinal tensile strength of composites and, therefore, should be incorporated in models.

8. Conclusions

This paper presented a benchmarking exercise comparing the results from three state–of–the–art models to predict tensile failure of FRPs, namely (i) an analytical *hierarchical scaling law* [14, 24], (ii) *direct numerical simulations* [15, 16, 19–23], and (iii) a *multiscale FE^2 model* [25–27]. This work leads to the following conclusions:

- There were significant discrepancies between the quantitative predictions from the three models, and different levels of correlation with experimental results, due to different model strategies and assumptions. These discrepancies occurred for all aspects of damage and failure — including ultimate strength, failure strain, non-linearity of stress–strain curves, and accumulation and clustering of fibre–breaks;

- Each of the three models has unique advantages. The *hierarchical scaling law* is computationally efficient and has a good correlation with experimental data. The *direct numerical simulation* method uses FE simulations for the stress concentrations, making it versatile to capture a wide range of mechanisms and features. The *multiscale FE^2 model* can be directly used in multi-scale FE simulations;

- "High–fidelity" models based on direct simulations are still not able to blind–predict the accumulation of fibre breakage and the failure of composites fibre–bundles as observed experi-

mentally with acceptable levels of accuracy. This suggests that we need to (i) further our understanding of the features governing longitudinal tensile failure of composites, (ii) refine the measurement of inputs for models (especially regarding the micromechanical properties of the fibres, matrix and interface), and (iii) carry out more blind comparisons between models and experiments.

This paper also illustrates the potential for improving the predictive capabilities of micromechanics–based models by benchmarking blind predictions from different approaches against state–of–the–art experimental techniques, focusing not only on the macroscopic material response (e.g. stress vs. strain curves and ultimate strength) but also on the underlying mechanisms (e.g. accumulation and clustering of fibre–breaks). The results of this exercise can guide further research to achieve a more fundamental understanding of the key failure mechanisms in composites, and to improve predictive capabilities; these steps are vital for developing improved materials, for designing efficient composite structures, and for assuring their continued performance while in service.

Acknowledgements

The authors gratefully acknowledge Luxfer Gas Cylinders Ltd., particularly Dr. Warren Hepples, and Airbus, for materials supply. The authors acknowledge the staff at the ID19/ESRF beamline in Grenoble, and Dr. Mavrogordato at the μ–VIS X-ray Imaging Centre, Southampton (launch funding via EPSRC Grant EP-H01506X). The authors also acknowledge several discussions in the scope of the UK Engineering and Physical Sciences Research Council Programme Grant EP/I02946X/1 on *High Performance Ductile Composite Technology*, a collaboration between Imperial College and the University of Bristol.

The work leading to this publication received funding from the European Union Seventh Framework Programme (FP7/2007-2013) under the topic NMP-2009-2.5-1, as part of the project HIVOCOMP (grant agreement nº 246389). The authors thank the Agency for Innovation by Science and Technology in Flanders (IWT) for grant funding for Y. Swolfs.

S. Pimenta acknowledges the support from the Royal Academy of Engineering for her Research Fellowship on *Multiscale discontinuous composites for large scale and sustainable structural applications* (2015–2019).

References

[1] M. J. Hinton and P. D. Soden. Predicting failure in composite laminates: the background to the exercise. *Composites Science and Technology*, 58(7):1001–1010, 1998.

[2] M. J. Hinton, A. S. Kaddour, and P. D. Soden. Evaluation of failure prediction in composite laminates: background to 'Part C' of the exercise. *Composites Science and Technology*, 64(3–4):321–327, 2004.

[3] A. S. Kaddour and M. J. Hinton. Maturity of 3D failure criteria for fibre-reinforced composites: Comparison between theories and experiments: Part B of WWFE-II. *Journal of Composite Materials*, 47(6-7):925–966, 2013.

[4] R. M. Christensen. The World Wide Failure Exercise II: Examination of Results. *Journal of Reinforced Plastics and Composites*, 32(21):1668–1672, 2013.

[5] A. Kaddour, M. Hinton, P. Smith, and S. Li. The background to the third world-wide failure exercise. *Journal of Composite Materials*, 47(20-21):2417–2426, 2013.

[6] S. L. Phoenix and I. J. Beyerlein. Statistical strength theory for fibrous composite materials. In A. Kelly, editor, *Comprehensive Composite Materials*, chapter 19, pages 559–639. Elsevier, Amsterdam, The Netherlands, 2000.

[7] S. Pimenta. Fibre failure modelling. In P. P. Camanho and S. Hallett, editors, *Numerical Modelling of Failure in Advanced Composite Materials*, chapter 8, pages 193–224. Woodhead Publishing, Cambridge, UK, 2015.

[8] Y. Swolfs, I. Verpoest, and L. Gorbatikh. A review of input data and modelling assumptions in longitudinal strength models for unidirectional fibre–reinforced composites. *Composite Structures*, 150:153–172, 2016.

[9] W. A. Curtin and N. Takeda. Tensile strength of fiber-reinforced composites: II. Application to polymer matrix composites. *Journal of Composite Materials*, 32(22):2060–2081, 1998.

[10] A. B. de Morais. Prediction of the longitudinal tensile strength of polymer matrix composites. *Composites Science and Technology*, 66(15):2990–2996, 2006.

[11] T. Okabe, M. Nishikawa, N. Takeda, and H. Sekine. Effect of matrix hardening on the tensile strength of alumina fiber-reinforced aluminum matrix composites. *Acta Materialia*, 54(9):2557–2566, 2006.

[12] J. Noda, M. Nakada, and Y. Miyano. Temperature dependence of accumulation of fiber breakages under tensile loading for unidirectional CFRP laminates. *Journal of Reinforced Plastics and Composites*, 27(10):1005–1019, 2008.

[13] T. Okabe, K. Ishii, M. Nishikawa, and N. Takeda. Prediction of tensile strength of unidirectional CFRP composites. *Advanced Composite Materials*, 19(3):229–241, 2010.

[14] S. Pimenta and S. T. Pinho. Hierarchical scaling law for the strength of composite fibre bundles. *Journal of the Mechanics and Physics of Solids*, 61(6), 2013.

[15] Y. Swolfs, R. M. McMeeking, I. Verpoest, and L. Gorbatikh. Matrix cracks around fibre breaks and their effect on stress redistribution and failure development in unidirectional composites. *Composites Science and Technology*, 108:16–22, 2015.

[16] Y. Swolfs, I. Verpoest, and L. Gorbatikh. Issues in strength models for unidirectional fibre-reinforced composites related to weibull distributions, fibre packings and boundary effects. *Composites Science and Technology*, 114:42–49, 2015.

[17] M. H. Berger and D. Jeulin. Statistical analysis of the failure stresses of ceramic fibres: Dependence of the Weibull parameters on the gauge length, diameter variation and fluctuation of defect density. *Journal of Materials Science*, 38(13):2913–2923, 2003.

[18] T. Fast, A. E. Scott, H. A. Bale, and B. N. Cox. Topological and euclidean metrics reveal spatially nonuniform structure in the entanglement of stochastic fiber bundles. *Journal of Materials Science*, 50(6):2370–2398, 2015.

[19] L. Li, S. V. Lomov, X. Yan, and V. Carvelli. Cluster analysis of acoustic emission signals for 2D and 3D woven glass/epoxy composites. *Composite Structures*, 116:286–299, 2014.

[20] Y. Swolfs, L. Gorbatikh, V. Romanov, S. Orlova, S. V. Lomov, and I. Verpoest. Stress concentrations in an impregnated fibre bundle with random fibre packing. *Composites Science and Technology*, 74:113–120, 2013.

[21] Y. Swolfs, L. Gorbatikh, and I. Verpoest. Stress concentrations in hybrid unidirectional fibre-reinforced composites with random fibre packings. *Composites Science and Technology*, 85:10–16, 2013.

[22] Y. Swolfs, R. M. McMeeking, I. Verpoest, and L. Gorbatikh. The effect of fibre dispersion on initial failure strain and cluster development in unidirectional carbon/glass hybrid composites. *Composites Part A — Applied Science and Manufacturing*, 69:279–287, 2015.

[23] Y. Swolfs, H. Morton, A. E. Scott, L. Gorbatikh, P. A. S. Reed, I. Sinclair, S. M. Spearing, and I. Verpoest. Synchrotron radiation computed tomography for experimental validation of a tensile strength model for unidirectional fibre-reinforced composites. *Composites Part A — Applied Science and Manufacturing*, 77:106–113, 2015.

[24] S. Pimenta. A computationally–efficient hierarchical scaling law to predict damage accumulation in composite fibre–bundles. *Composites Science and Technology*, 146:210–225, 2017.

[25] F. Feyel. A multilevel finite element method (FE2) to describe the response of highly non-linear structures using generalized continua. *Computer Methods in applied Mechanics and Engineering*, 192:3233–3244, 2003.

[26] F. V. Souza, D. H. Allen, and Y. R. Kim. Multiscale model for predicting damage evolution in composites due to impact loading. *Composites Sciences and Technology*, 68:2624–2634, 2008.

[27] A. Thionnet and J. Renard. Multi-scale analysis to determine fibre/matrix debonding criteria in sic/titanium composites with and without consideration of the manufacturing residual stresses. *Composites Science and Technology*, 58:945–955, 1998.

[28] A. E. Scott, I. Sinclair, S. M. Spearing, A. Thionnet, and A. R. Bunsell. Damage accumulation in a carbon/epoxy composite: Comparison between a multiscale model and computed tomography experimental results. *Composites Part A — Applied Science and Manufacturing*, 43:1514–1522, 2012.

[29] P. Wright, A. Moffat, I. Sinclair, and S. M. Spearing. High resolution tomographic imaging and modelling of notch tip damage in a laminated composite. *Composites Science and Technology*, 70(10):1444–1452, 2010.

[30] A. E. Scott, M. Mavrogordato, P. Wright, I. Sinclair, and S. M. Spearing. In situ fibre fracture measurement in carbon-epoxy laminates using high resolution computed tomography. *Composites Science and Technology*, 71(12):1471–1477, 2011.

[31] Toray Carbon Fibers America, Inc. Torayca T800H Data Sheet — Technical Data Sheet No. CFA-007. http://www.toraycfa.com/pdfs/T800HDataSheet.pdf, last accessed December 2012.

[32] A. S. Kaddour, M. J. Hinton, P. A. Smith, and S. Li. Mechanical properties and details of composite laminates for the test cases used in the third world–wide failure exercise. *Journal of Composite Materials*, 47:2427–2442, 2013.

[33] F. Tanaka, T. Okabe, H. Okuda, I. A. Kinloch, and R. J. Young. Factors controlling the strength of carbon fibers in tension. *Composites Part A — Applied Science and Manufacturing*, 57:88–94, 2014.

[34] Hexcel Coorporation. HexPly M21 Product Data — Publication FTA002c, March 2007.

[35] T. Hobbiebrunken, B. Fiedler, M. Hojo, and M. Tanaka. Experimental determination of the true epoxy resin strength using micro-scaled specimens. *Composites Part A — Applied Science and Manufacturing*, 38(3):814–818, 2007.

[36] E. M. Odom and D. F. Adams. Specimen size effect during tensile testing of an unreinforced polymer. *Journal of Materials Science*, 27(7):1767–1771, 1992.

[37] W. I. Newman and A. M. Gabrielov. Failure of hierarchical distributions of fiber–bundles. 1. *International Journal of Fracture*, 50(1):1–14, 1991.

[38] A. Kelly and W. R. Tyson. Tensile properties of fibre–reinforced metals: Copper/tungsten and copper/molybdenum. *Journal of the Mechanics and Physics of Solids*, 13(6):329–338, 1965.

[39] M. R Wisnom and D. Green. Tensile failure due to interaction between fibre breaks. *Composites*, 26:499–508, 1995.

[40] T. Okabe, H. Sekine, K. Ishii, M. Nishikawa, and N. Takeda. Numerical method for failure simulation of unidirectional fiber-reinforced composites with spring element model. *Composites Science and Technology*, 65(6):921–933, 2005.

[41] Y. Swolfs, I. Verpoest, and L. Gorbatikh. Maximising the hybrid effect in unidirectional hybrid composites. *Materials & Design*, 93:39–45, 2016.

[42] M. R. Wisnom, G. Czel, Y. Swolfs, M. Jalalvand, L. Gorbatikh, and I. Verpoest. Hybrid effects in thin ply carbon/glass unidirectional laminates: Accurate experimental determination and prediction. *Composites Part A — Applied Science and Manufacturing*, 93:39–45, 2016.

[43] M. R. Nedele and M. R. Wisnom. Three dimensional finite analysis of the stress concentration at a single fibre break. *Composites Science and Technology*, 51(4):517–524, 1994.

[44] P. W. J. Van den Heuvel, M. K. Wubbolts, R. J. Young, and T. Peijs. Failure phenomena in two–dimensional multi–fibre model composites: 5. A finite element study. *Composites Part A — Applied Science and Manufacturing*, 29(9-10):1121–1135, 1998.

[45] J. M. Lifschitz and A. Rotem. Time-dependent longitudinal strength of unidirectional fibrous composites. *Fibre Science and Technology*, 3(1):1–20, 1970.

[46] D. C. Lagoudas, C. Y. Hui, and S. L. Phoenix. Time evolution of overstress profiles near broken fibers in a composite with a viscoelastic matrix. *International Journal of Solids and Structures*, 25(1):45–66, 1989.

[47] I. J. Beyerlein, C. H. Zhou, and L. S. Schadler. Time evolution of stress redistribution around multiple fiber breaks in a composite with viscous and viscoelastic matrices. *International Journal of Solids and Structures*, 35(24):3177–3211, 1998.

[48] J. Lee, C. E. Harris, and D. H. Allen. nternal state variable approach for predicting stiffness reduction in fibrous laminated composites with matrix cracks. *Journal of Composite Materials*, 23(12):1273–1291, 1989.

[49] H. Y. Chou, A. R. Bunsell, G. Mair, and A. Thionnet. Effect of the loading rate on ultimate strength of composites. Application: Pressure vessel slow burst test. *Composites Structures*, 104:144–153, 2013.

[50] H. Y. Chou, A. Thionnet, A. Mouritz, and A. R. Bunsell. Stochastic factors controlling the failure of carbon/epoxy composites. *Journal of Materials Science*, 51 (50th anniversary number):311–333, 2015.

[51] A. Thionnet, H. Y. Chou, and A. R. Bunsell. Fibre break processes in unidirectional composites. *Composites Part A — Applied Science and Manufacturing*, 65:148–160, 2014.

[52] A. Thionnet, H. Y. Chou, and A. R. Bunsell. Fibre break failure processes in unidirectional composites. Part 1: Failure and critical damage state induced by increasing tensile loading. *Applied Composite Materials*, 24:119–140, 2015.

[53] S. Blassiau. Modélisation des phénomènes microstructuraux au sein d'un composite unidirectionnel carbone/époxy et prédiction de durée de vie: contrôle et qualification de réservoirs bobinés. *Thèse, Ecole des Mines de Paris*, 2005.

[54] H. Y. Chou, H. Zejli, A. Thionnet, A. Bunsell, A. Mouritz, and M. Bannister. Détection et discrimination par émission acoustique des endommagements dans les composites stratifiés d'unidirectionnels: rupture de fibre, macro et microfissuration intralaminaire, microdélaminage. Comparaison expérience/modélisation. In *Matériaux 2010*, Nantes, France, 2010.

[55] S. Blassiau, A. Thionnet, and A. Bunsell. Micromechanisms of load transfer in a unidirectional carbon-fibre epoxy composite due to fibre failures. Part 1: Micromechanisms and 3D analysis of load transfer, the elastic case. *Composite Structures*, 74:303–318, 2006.

[56] C. Baxevanakis. Comportement statistique à rupture des composites stratifiés. *Thèse, Ecole des Mines de Paris*, 1994.

[57] S. Blassiau, A. Thionnet, and A. Bunsell. Micromechanisms of load transfer in a unidirectional carbon-fibre epoxy composite due to fibre failures. Part 2: Influence of viscoelastic and plastic matrices on the mechanism of load transfer. *Composite Structures*, 74:319–331, 2006.

[58] S. Blassiau, A. Thionnet, and A. Bunsell. Micromechanisms of load transfer in a unidirectional carbon-fibre epoxy composite due to fibre failures. Part 3: Multiscale reconstruction of composite behaviour. *Composite Structures*, 83:312–323, 2008.

[59] H. Morton. *3D imaging of the tensile failure mechanisms of carbon fibre composites*. PhD thesis, University of Southampton, 2014.

[60] J. Schindelin, I. Arganda–Carreras, E. Frise, V. Kaynig, M Longair, T Pietzsch, S. Preibisch, C Rueden, S Saalfeld, B Schmid, J.–Y. Tinevez, D. J. White, V. Hartenstein, K. Eliceiri, P. Tomancak, and A. Cardona. Fiji: an open–source platform for biological–image analysis. *Nature Methods*, 9(7):676–682, 2012.

[61] A. B. de Morais. Stress distribution along broken fibres in polymer–matrix composites. *Composites Science and Technology*, 61(11):1517–1580, 2001.

[62] I. J. Beyerlein and S. L. Phoenix. Stress concentrations around multiple fiber breaks in an elastic matrix with local yielding or debonding using quadratic influence superposition. *Journal of the Mechanics and Physics of Solids*, 44(12):1997–2039, 1996.

[63] M. L. Accorsi, A. Pegoretti, and A. T. Dibenedetto. Dynamic analysis of fibre breakage in single– and multiple–fibre composites. *Journal of Materials Science*, 31(16):4181–4187, 1996.

[64] S. L. Phoenix and R. G. Sexsmith. Clamp effects in fiber testing. *Journal of Composite Materials*, 6:322–337, 1972.

[65] J. Watanabe, F. Tanaka, H. Okuda, and T. Okabe. The tensile strength distribution of carbon fibers at short gauge length. *Advanced Composite Materials*, 23(5-6):535–550, 2014.

[66] E. G. Stoner, D. D. Edie, and S. D. Durham. An end–effect model for the single–filament tensile test. *Journal of Materials Science*, 29(24):6561–6574, 1994.

[67] G. M. Vyas, S. T. Pinho, and P Robinson. Constitutive modelling of fibre-reinforced composites with unidirectional plies using a plasticity-based approach. *Composites Science and Technology*, 71(8):1068–1074, 2011.

[68] G. Catalanotti, P. P. Camanho, and A. T. Marques. Three-dimensional failure criteria for fiber-reinforced laminates. *Composite Structures*, 93:63–79, 2013.

[69] D. R. B. Aroush, E. Maire, C. Gauthier, S. Youssef, P. Cloetens, and H. D. Wagner. A study of fracture of unidirectional composites using in situ high-resolution synchrotron X-ray microtomography. *Composites Science and Technology*, 66(10):1348–1353, 2006.

[70] R. Ganesh, S. Sockalingam, B. Z. Haque, and J. W. Gillespie. Dynamic effects of single fiber break in unidirectional glass fiber-reinforced composites. *Journal of Composite Materials*, 51(9):1307–1320, 2017.

[71] J. Henry and S. Pimenta. Semi-analytical simulation of aligned discontinuous composites. *Composites Science and Technology*, 144:230–244, 2017.

Table 1: Contributors to this publication reporting the benchmarking exercise.

Institution	Contributor(s)	Contribution
KU Leuven	Yentl Swolfs Larissa Gorbatikh	Predictions using *direct numerical simulations* [15, 16, 19–23]
Imperial College London	Soraia Pimenta	Predictions using a *hierarchical scaling law* [14, 24]
University of Southampton	Hannah Morton Mark Spearing Ian Sinclair	Input data and experimental results
Mines ParisTech	Alain Thionnet Anthony Bunsell	Predictions using a *multiscale FE^2 model* [25–28]

Table 2: Input data provided for modelling the hypothetical composite in Case I. A Weibull distribution was assumed for the strength of individual fibres, with cumulative distribution function $F(\sigma) = 1 - \exp\left[-(\sigma/\sigma_0)^m\right]$ (where m is the Weibull modulus, σ_0 is the scale parameter, and σ is the applied stress).

Geometry and elastic constants of fibres		Fibre strength distribution	
Fibre diameter	12 µm	Weibull modulus	8.0
Young's modulus	100 GPa	Scale parameter	3000 MPa
Poisson's ratio	0.2	Gauge length	1.0 mm
Matrix/interface–dominated properties		Composite geometry	
Matrix Young's modulus	10 GPa	Fibre volume fraction	50%
Composite interlaminar shear strength	50 MPa	Gauge length of specimen	1.0 mm
Matrix Poisson's ratio	0.3	No. fibres in cross section	2000

Table 3: Input data provided for modelling the T800/M21 composite in Case II. A Weibull distribution (see expression in Table 2) was assumed for the strength of individual fibres.

Geometry and elastic constants of fibres [31, 32]			
Fibre diameter	5 µm	Transverse Young's modulus	19 GPa
Longitudinal Young's modulus	294 GPa	Longitudinal shear modulus	27 GPa
Longitudinal Poisson's ratio	0.2	Transverse shear modulus	7 GPa
Fibre strength distribution [33]		Matrix/interface–dominated properties [34]	
Weibull modulus	4.8	Matrix Young's modulus	3.5 GPa
Scale parameter	3900 MPa	Composite interlaminar shear strength	96 MPa
Gauge length	100 mm	Matrix Poisson's ratio	0.3
Composite geometry [measured]			
Fibre volume fraction	55%	Number of fibres in cross section	5500
Gauge length of specimen	1.54 mm		

Table 4: Summary of the different modelling approaches used in this exercise.

		Hierarchical scaling law (Sec. 4.1)	Direct numeric. simulation (Sec. 4.2)	Multiscale FE^2 model (Sec. 4.3)
Model framework		Analytical formulation based on a hierarchical scaling law, coupling statistics with shear–lag	Monte-Carlo simulations of a FBM, coupled with FE simulations for stress concentrations	Monte-Carlo simulations of FE macro–models, coupled with RVE FE micro–models for the local response
Material response of constituents	Fibres	Isotropic; linear–elastic up to failure; Weibull scaling of strength to the recovery length under a non-uniform stress field	Transversely isotropic in FE and isotropic in FBM; linear–elastic up to failure; Weibull scaling of strength to the length of a fibre radius	Transversely isotropic; linear–elastic up to failure; Weibull scaling of strength to 4 mm long fibres under a uniform stress field
	Matrix	Perfectly–plastic	Elastic or elasto–plastic	Viscoelastic
	Fibre–matrix interface	Perfectly–plastic (combined with matrix response)	Perfectly bonded	With most detrimental debonding
Fibre packing		Square	Random	Square
Stress concentrations	Near individual fibre breaks	Stress concentration factor of 2 in the nearest surviving fibre (from shear–lag)	Library of stress concentrations from FE simulations of RVEs with one central broken fibre	Library of stress concentrations from FE simulations of RVEs with one broken fibre, out of 32
	Near broken clusters	Stress concentration factor of 2 in the nearest surviving cluster (from shear–lag)	Superposition of stress concentrations for individual fibre breaks	Library of stress concentrations from FE simulations of RVEs with 2, 4, 8 or 16 broken fibres, out of 32
Clusters of broken fibres	Definition of cluster with n_{clust} broken fibres	Combination of two clusters with $n_{\text{clust}}/2$ breaks within a control volume (i.e. with interacting recovery regions)	n_{clust} fibre–breaks within an axial distance of 10 fibre radii and within a lateral distance of 4 fibre radii (measured between fibre–centres)	n_{clust} broken fibres within a RVE (with 32 fibres, 4 mm long)
	Possible cluster sizes (no. fibres)	1, 2 to 3, 4 to 7, 8 to 15, ...	Any positive integer	1, 2, 4, 8, ...
	Co-planarity of fibre–breaks	Stress fields assume co-planar breaks in each cluster	No assumption of co-planar breaks	Stress fields assume co-planar breaks in each RVE
Results for composites	Determination of the failure point	Expected value of strength calculated from the full survival probability distribution (Eq. 1)	Stress corresponding to an exponential growth of fibre breaks, which indicates a critical cluster	Stress corresponding to an instability (first knee) in the stress–strain curve (see Figure 3)
	Non–linearity in the stress–strain curves	Expected strains and loss of stiffness calculated from the expected density of broken fibres and clusters	The stress–strain curve of the composite is assumed to be linear–elastic	Macro–level strains include a loss of stiffness equal to the ratio of broken fibres in each RVE

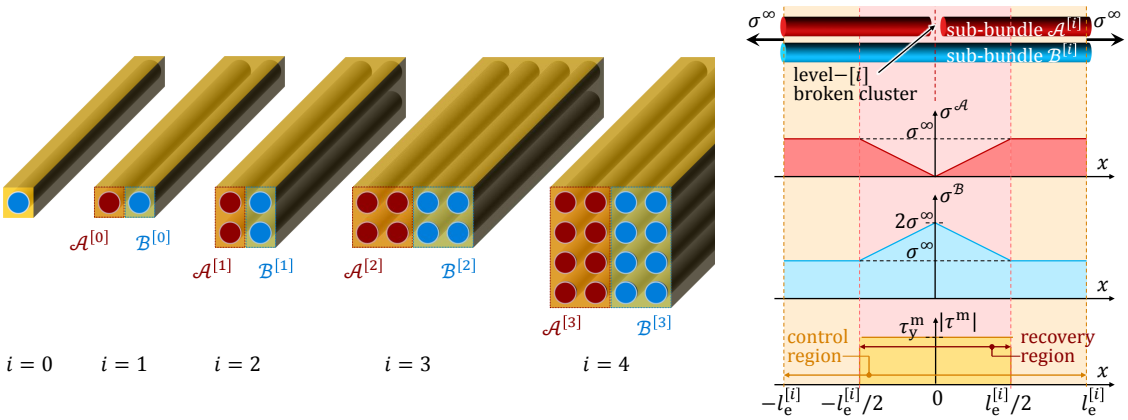

(a) Hierarchical composite fibre bundles.

(b) Stress fields in a level–$[i+1]$ bundle, after the formation of a level-$[i]$ broken cluster.

Figure 1: Overview of the analytical *hierarchical scaling law* [14, 24].

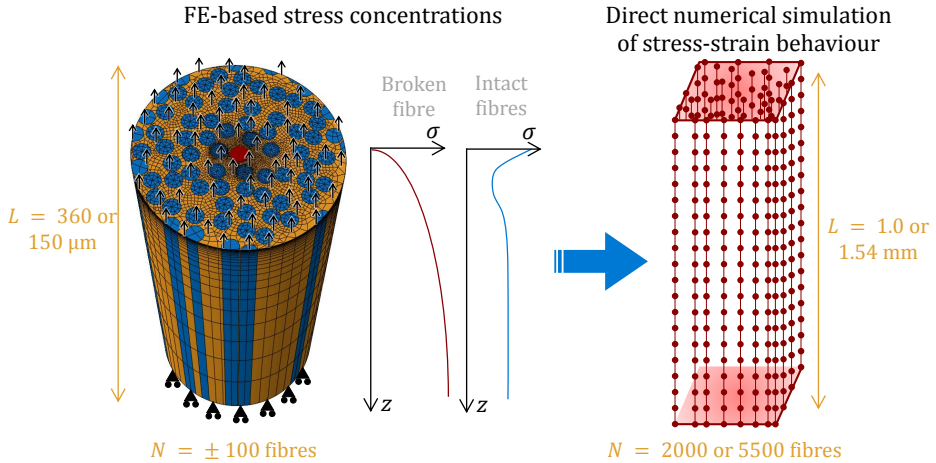

Figure 2: Overview of the *direct numerical simulation* method [15, 16, 19–23].

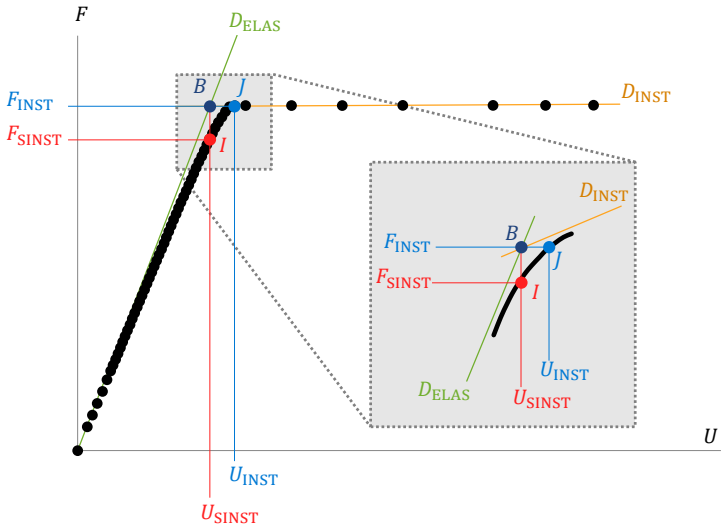

Figure 3: The experimental failure of a structure is defined as a break of the structure into two parts. For the *multiscale FE^2 model* it appears as a point of INSTability (J, the failure point) in the load (F) vs. displacement (U) curve. In the cases considered here, because of the difficulty in controlling the failure process, J is difficult to observe. For this reason, a "Start of INSTability" point (denoted as I) has also be defined. The way these points can be found has been explained in detail elsewhere [52].

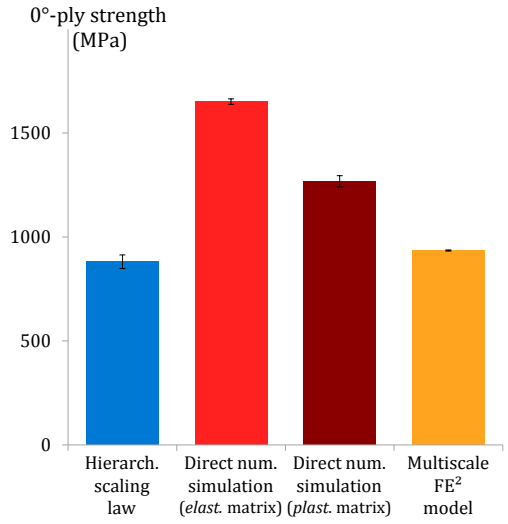

(a) 0°–ply strength.

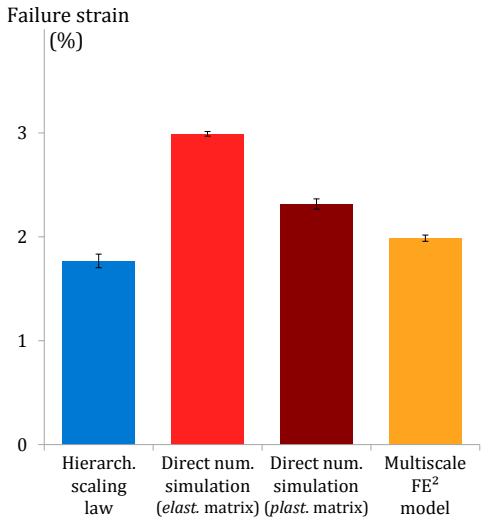

(b) Failure strain.

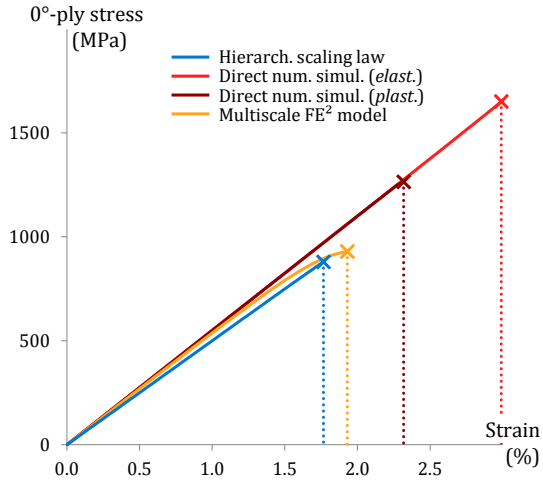

(c) Representative 0°–ply stress vs. strain curves.

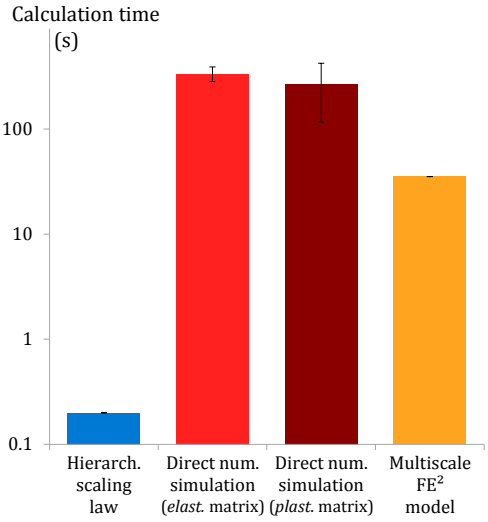

(d) Computational clock time.

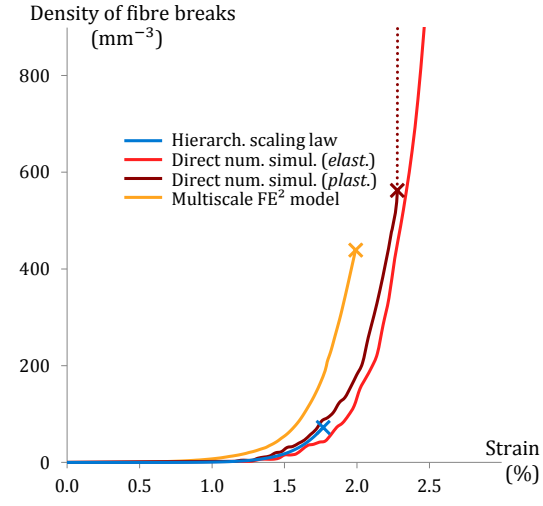

(e) Total density of fibre breaks.

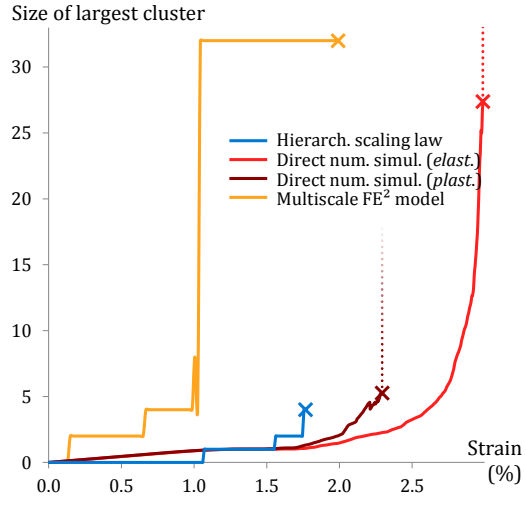

(f) Evolution of the size (no. fibres) of the largest cluster.

Figure 4: Model predictions for Case I. Error bars represent ± one standard deviation. Predicted failure is highlighted with a cross (×), and the post-failure unstable response is shown in dotted lines (in subfigures **(c)**, **(e)** and **(f)**.

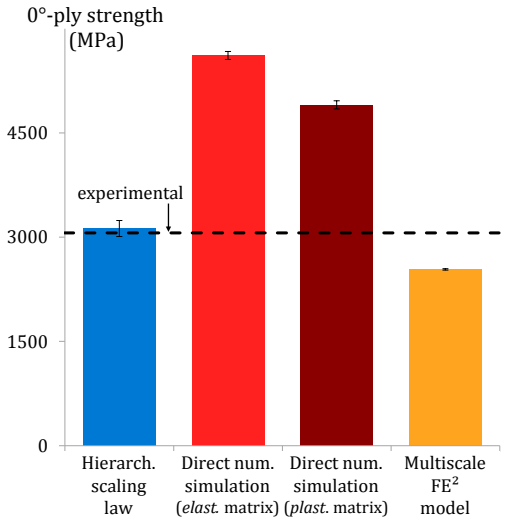

(a) 0°–ply strength.

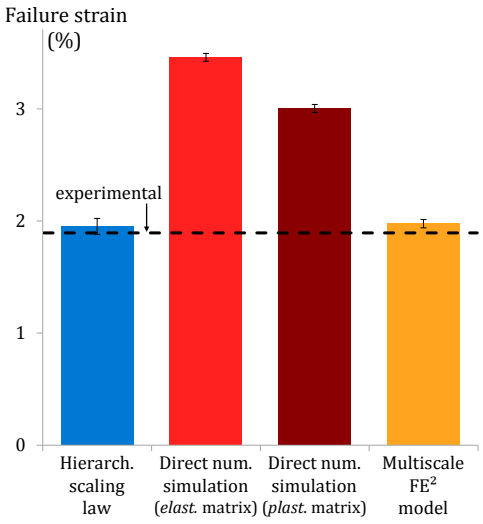

(b) Failure strain.

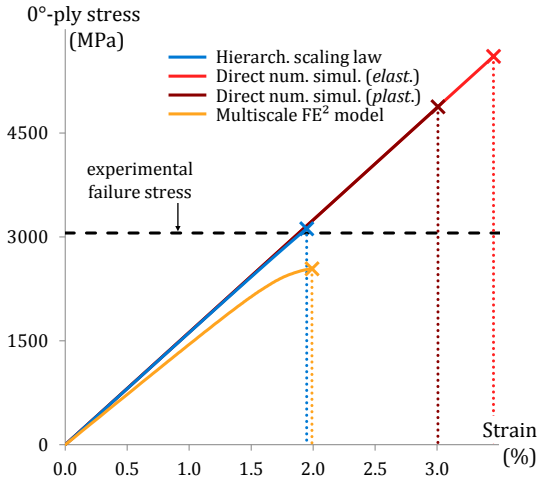

(c) Representative 0°–ply stress vs. strain curves.

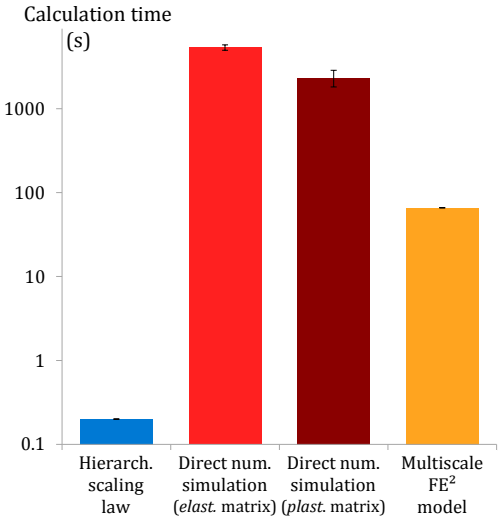

(d) Computational clock time.

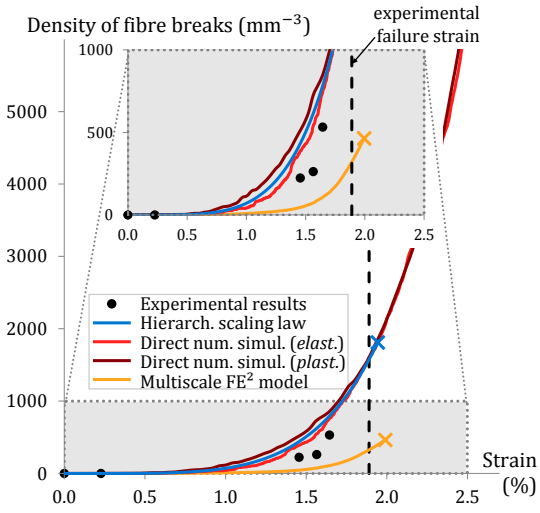

(e) Total density of fibre breaks.

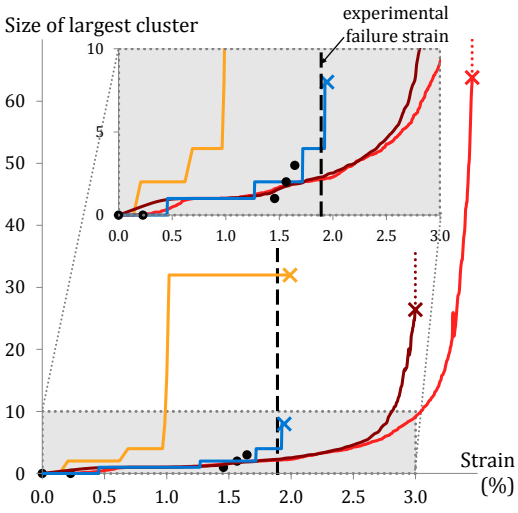

(f) Evolution of the size (no. fibres) of the largest cluster (same caption as in subfigure **(e)**.)

Figure 5: Model predictions for Case II. Error bars represent ± one standard deviation. Predicted failure is highlighted with a cross (×), and the post-failure unstable response is shown in dotted lines (in subfigures **(c)**, **(e)** and **(f)**.